ACS Energy LETTERS

http://pubs.acs.org/journal/aelccp

High-Power Hybrid Solid-State Lithium–Metal Batteries Enabled by Preferred Directional Lithium Growth Mechanism

Sewon Kim,[○] Gabin Yoon,[○] Sung-Kyun Jung, SeonTae Park, Ju-Sik Kim, Kyungho Yoon, Sunyoung Lee, and Kisuk Kang*

Cite This: *ACS Energy Lett.* 2023, 8, 9–20

Read Online

ACCESS | Metrics & More | Article Recommendations | Supporting Information

ABSTRACT: **Solid electrolytes are revolutionizing the field of lithium–metal batteries; however, their practical implementation has been impeded by the interfacial instability between lithium metal electrodes and solid electrolytes. While various interlayers have been suggested to address this issue in recent years, long-term stability with repeated lithium deposition/stripping has been challenging to attain. Herein, we successfully operate a high-power lithium–metal battery by inducing the preferred directional lithium growth with a rationally designed interlayer, which employs (i) crystalline-direction-controlled carbon material providing isotropic lithium transports, with (ii) prelithium deposits that guide the lithium nucleation direction toward the current collector. This combination ensures that the morphology of the interlayer is mechanically robust while regulating the preferred lithium growth underneath the interlayer without disrupting the initial interlayer/electrolyte interface, enhancing the durability of the interface. We illustrate how these material/geometric optimizations are conducted from the thermodynamic considerations, and its applicability is demonstrated for the garnet-type $Li_{7-x}La_{3-a}Zr_{2-b}O_{12}$ (LLZO) solid electrolytes paired with the capacity cathode. It is shown that a lithium–metal cell with the optimized amorphous carbon interlayer with prelithium deposits exhibits outstanding room-temperature cycling performance (99. 6% capacity retention after 250 cycles), delivering 4.0 mAh cm^{-2} at 2.5 mA cm^{-2} without significant degradation of the capacity. The successful long-term operation of the hybrid solid-state cell at room temperature (approximately a cumulative deliverable capacity of over 1000 mAh cm^{-2}) is unprecedented and records the highest performance reported for lithium–metal batteries with LLZO electrolytes until date.**

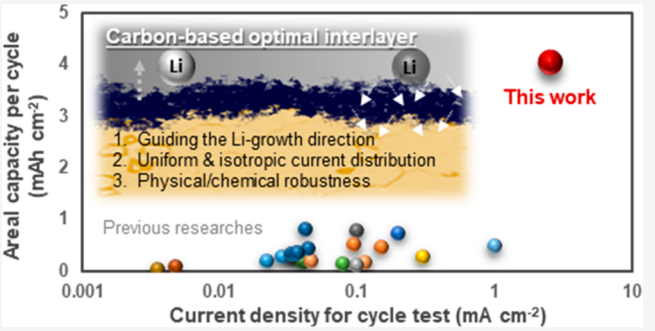

Solid-state batteries using lithium metal anodes and solid electrolytes are considered promising alternatives to the current lithium-ion batteries because they are safe and can potentially exhibit high energy densities.[1−7] Among the various solid electrolytes proposed so far, garnet-type oxide electrolytes (such as $Li_7La_3Zr_2O_{12}$ (LLZO)) are some of the leading candidates for lithium–metal solid-state batteries due to their high ionic conductivities at room temperature (~1 mS cm^{-1}) and chemical stability with lithium metal.[3,8−11] However, their real-world implementation has been hampered by the premature short-circuiting caused by lithium metal piercing through the LLZO under practical current densities.[12−14] Various mechanisms have been suggested as causes of this phenomenon and are currently under extensive investigations;[7,15−18] however, the interfacial inhomogeneity/instability occurring between lithium metal anode and LLZO has been considered as the most crucial attribute.

Many studies have reported that the internal short circuits can be caused by the localized electrodeposition arising from the inhomogeneous interfacial nature, which is typically induced by the poor contact of lithium metal with LLZO and intrinsically low lattice–lithium diffusivity in dynamic lithium stripping and deposition processes.[5,14,19−21] As illustrated in Figure 1a, the ill-defined interface can induce the inhomogeneous current distribution and the localized lithium plating, which trigger a rapid lithium penetration into

Received: September 21, 2022
Accepted: November 10, 2022

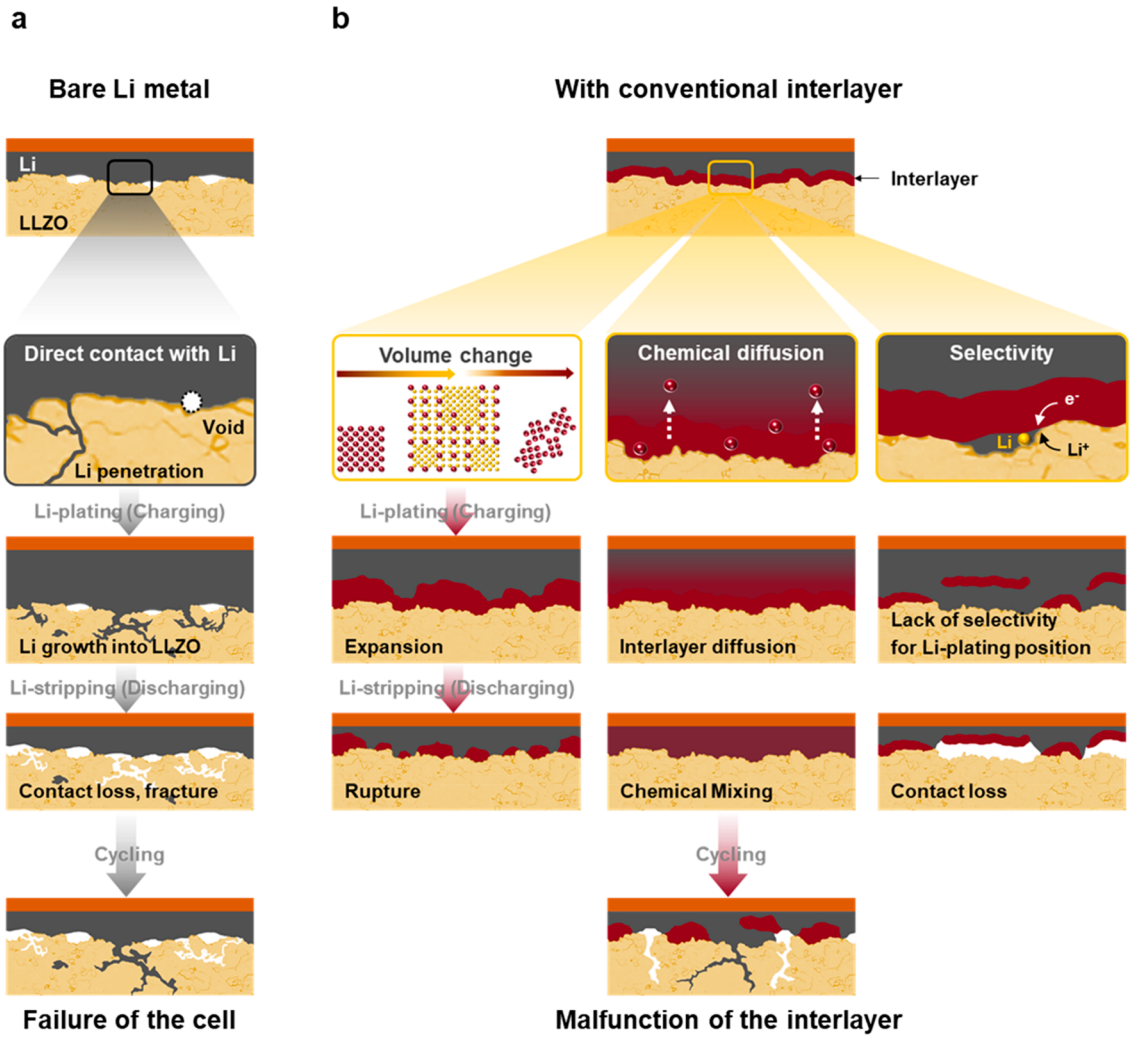

Figure 1. Schematic illustrations of the degradation mechanism at the interface of a solid electrolyte and a lithium−metal anode during repetitive lithium plating and stripping. (a) On application of bare lithium metal, pronounced lithium metal penetration and void formation from the beginning of cell operation. (b) Failure of the cell on using bare lithium metal initially retarded using conventional interlayers. However, (electro)chemical/physical instability of the interlayer (attributed to large volume change, chemical mixing/dissolution of the interlayer into the lithium metal, and the lack of lithium-plating-position control) eventually causes failure of the cells, as illustrated in the diagrams.

the electrolyte through the grain boundaries, or by crack propagation.[18,22] It is further aggravated during the lithium stripping process due to the morphological instability at the interface involving the lithium void, which tends to be formed due to the sluggish lattice−lithium diffusion compared with the applied current density, eventually causing lithium metal penetration into the electrolyte.[20,21,23,24] For the past several years, researchers found that introducing an interlayer between the LLZO electrolyte and lithium metal anode could improve the interfacial homogeneity and stability.[19,23,25−30] Various compounds such as metallic alloys, oxides, nitrides, and halides were proposed as promising interlayers on the LLZO with the enhanced wettability with lithium metal and the high lithium ionic conduction that allows the homogeneous lithium flux.[5,25−28,31−43] In particular, metallic interlayers that can alloy with lithium were demonstrated to be markedly effective; it promotes not only the wettability with the LLZO but also the lattice−lithium diffusion in the alloying matrix, successfully homogenizing the lithium-ion flux distribution even during the high-rate stripping process.[31,34,44,45]

Nevertheless, it has been arduous to achieve acceptable long-term performance for practical applications due to the limitations of the interlayers proposed so far. It is typically attributable to degradation of the interlayer itself during long-term operation of batteries, depending on its working mechanism, as schematically illustrated in Figure 1b. The widely reported alloying interlayers (e.g., gold, silver, germanium, and silicon) are often accompanied by significant volume change during alloying/dealloying, and the repeated deposition/stripping of lithium constantly degenerates the original morphology of the interlayer.[5,26,28,30−33] It ultimately causes the rupture of the interlayer coated on LLZO, exposing the naked LLZO interface to the lithium metal, failing in the role of the interlayer. Similar degradations are also expected for oxide-based or nitride-based interlayers, which can undergo conversion reaction with lithium metal.[35,36,39,46,47] Such conversion reactions generally yield a significant morphological change upon repeated lithium uptake, continuously deteriorating the interlayer stability. Moreover, the alloys that can homogenize the lithium-ion flux such as gold and silver are

https://doi.org/10.1021/acsenergylett.2c02150
ACS Energy Lett. 2023, 8, 9−20

Table 1. Calculated Interfacial Energies According to the Lithium Plating Position and Interlayer Materials (See Supporting Information Note S1 and Figure S1 for Details)

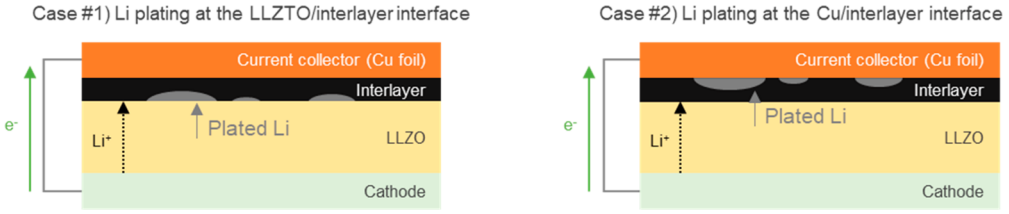

	Calculated interface energy (J m^{-2})			
	Case #1[a]	Case #2[b]		
Interlayer material	(Collector/interlayer) + (Li/LLZTO)	(Collector/Li) + (interlayer/LLZTO)	Preferential behavior	Volume expansion (%)
LiC_6 (001)	(−0.554) + (−0.708) = −1.362	(−1.485) + (−0.354) = −1.839	Case #2	+11
W (110)	(−3.363) + (−0.708) = −4.071	(−1.485) + (−2.002) = −3.487	Case #1	
LiF (001)	(−0.716) + (−0.708) = −1.424	(−1.485) + (−0.781) = −2.266	Case #2	0
Li_3Au (001)	(−1.555) + (−0.708) = −2.263	(−1.485) + (−1.296) = −2.781	Case #2	+245
Li_9Ag_4 (001)	(−1.373) + (−0.708) = −2.081	(−1.485) + (−1.353) = −2.838	Case #2	+211
Li_5Si_2 (001)	(−1.319) + (−0.708) = −2.027	(−1.485) + (−1.286) = −2.771	Case #2	+133

[a]Case #1: Li plating between LLZO and the interlayer. [b]Case #2: Li plating between the current collector and the interlayer.

vulnerable to the chemical diffusion into the lithium matrix upon its contact.[48,49] The alloying element is likely to diffuse out from the interface into the lithium bulk region over time, gradually losing its interlayer role during long-term operation of the battery. Another aspect that has been often overlooked is the lack of the selectivity in the lithium deposition with respect to the interlayer position. While lithium is supposed to be deposited between the current collector and the interlayer, some electrically conductive interlayers may allow the lithium deposition between the interlayer and the LLZO, as schematically illustrated in the right panel of Figure 1b. Even slight electrical leakage through the thin interlayer may induce the lithium nucleation underneath the interlayer, inducing the detachment of the interlayer from the LLZO surface and its deterioration.

In this study, we focus on how to design an optimal interlayer, rationally considering these degradation mechanisms of the interlayer upon the lithium plating and stripping. Based on the thermodynamic properties of the candidate materials estimated by density functional theory (DFT) calculations, a carbon-based material is selected as the core component of the interlayer, which can preferentially induce lithium plating between the current collector (copper) and the interlayer. In this consideration, it is also unveiled that the crystalline orientations of the carbon domains are important in homogenizing the lithium-ion flux through the interlayer, indicating the necessity in the crystalline engineering of carbon. Additionally, it is shown that the high kinetic energy barrier for lithium nucleation can be effectively lowered with the aid of the prelithium deposits, which further facilitate the preferred lithium growth without destructing the original interlayer/electrolyte interface. Through the series of in-depth characterizations, we demonstrate that this rational selection is quite effective, which allows the long-term stability of the interlayer not only in the morphology but also in securing the reversible lithium stripping/deposition. We fabricate a high-capacity hybrid solid-state cell with an NCA811 ($LiNi_{0.8}Co_{0.1}Al_{0.1}O_2$) cathode, employing the optimized carbon interlayer between an LLZO electrolyte and lithium metal anode, and validate that it exhibits remarkable room-temperature cycling performance over 250 cycles with 99.6% capacity retention, delivering 4.0 mAh cm^{-2} at 2.5 mA cm^{-2} with a cumulative capacity of over 1000 mAh cm^{-2}. The successful long-term operation at record-high 2.5 mA cm^{-2} at room temperature paves a new pathway toward the development of practical all-solid-state lithium metal batteries.

Material Selection through Thermodynamic Calculations. In designing the optimal interlayer, several criteria were established considering the underlying mechanisms of short-circuit formation in the cell, as illustrated in Figure 1. We reasoned that the interlayer should be able to (1) provide an intimate contact both with the LLZO electrolyte and with lithium metal, (2) act as a buffer layer for lithium redistribution to mitigate current inhomogeneity at the interface, and (3) sustain its physical and chemical stability guiding the lithium deposition during the long-term cycling. Given these criteria, the suitability of several candidate materials was first screened based on their thermodynamic preferences with respect to the position of lithium plating at the interface (i.e., between current collector (copper) and LLZO (case #1) vs between interlayer and LLZO (case #2)), as illustrated in Table 1. The preferential position of lithium was determined by comparing the interfacial energies of respective copper/interlayer/LLZO systems from DFT calculations (see Supporting Information Note S1, Figures S1 and S2, and Table S1 for details). Table 1 compares the interfacial energies of candidate interlayer materials in these two cases. It indicates that the lithium metal plating can occur preferentially either at the interlayer/current collector or interlayer/LLZO interface depending on the interlayer species. With a tungsten interlayer applied, lithium metal was predicted to be plated between the electrolyte and the interlayer, which infers the likelihood of the detachment of the tungsten interlayer from the LLZO. On the other hand, interlayer candidates such as LiF, Ag, Au, Si, and carbon could help on the preferential lithium plating toward the current collector, indicating the morphological stability.

Metallic interlayers such as Ag, Au, and Si were, however, found to undergo a substantially large volume change upon contact with lithium metal along with the potential risk of the dilution in the lithium matrix, indicating that they would not retain their original morphology after repetitive lithium plating

https://doi.org/10.1021/acsenergylett.2c02150
ACS Energy Lett. 2023, 8, 9−20

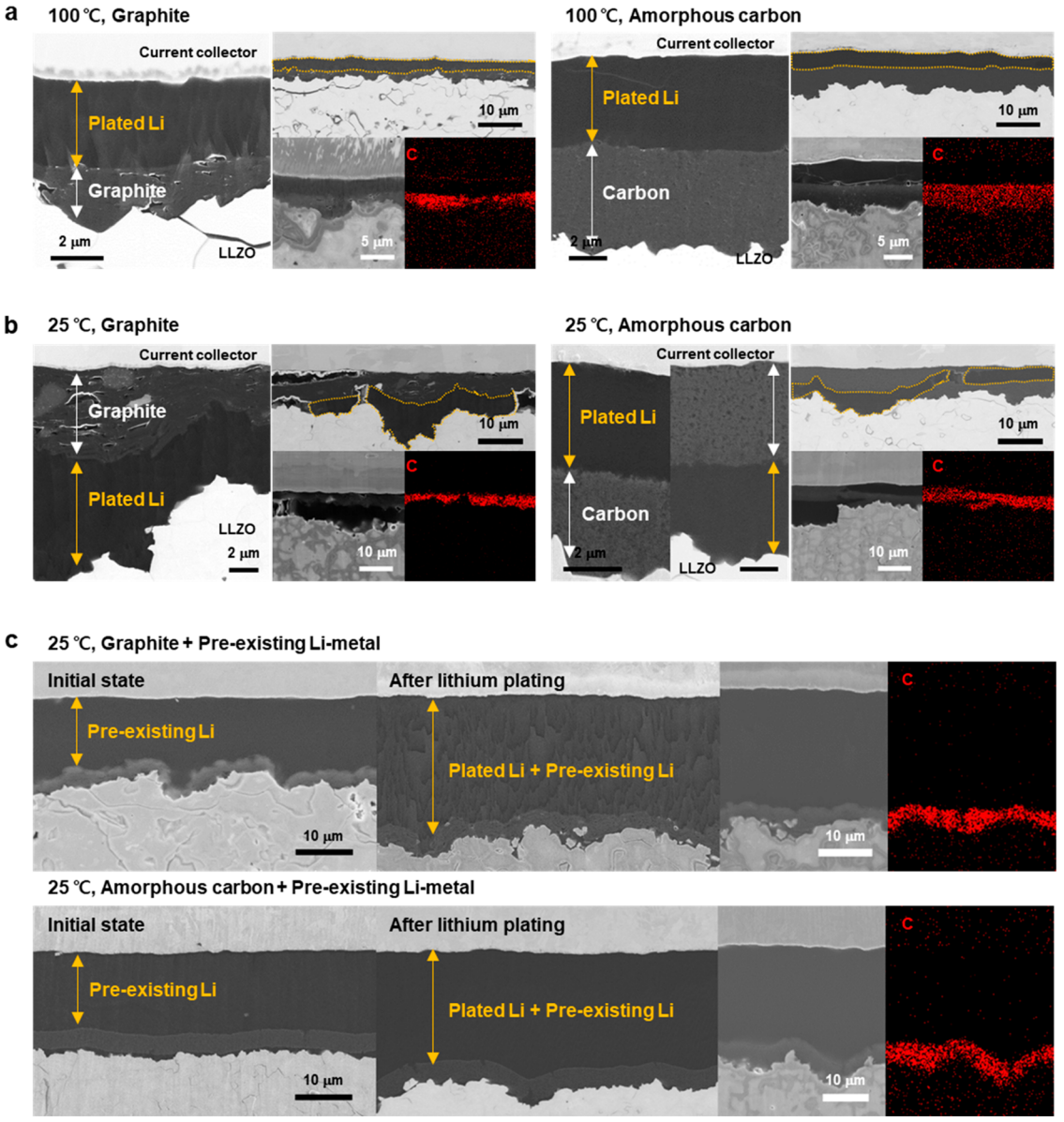

Figure 2. Lithium-plating behaviors through the graphite or amorphous carbon layer under various conditions. Cross-sectional SEM and EDS images of the LLZO solid electrolyte/anode interfaces after electrodeposition of lithium at various magnifications scaling (a, b) to the (left) graphite layer and (right) amorphous carbon layer at 100 and 25 °C, respectively, and (c) through the graphite interlayer or amorphous carbon interlayer with the pre-existing lithium metal at 25 °C. (a) At 100 °C, lithium was plated between the carbon layer (graphite or amorphous) and the current collector. In panel b, at 25 °C, lithium was randomly plated either between the carbon interlayer and the solid electrolyte, or between the carbon interlayer and the current collector, indicating the loss of the lithium deposition preferential position. In panel c, the entire lithium was plated on the pre-existing lithium metal seed layer after passing through the interlayer, regardless of the type of carbon used.

and stripping (Figure S3).[5,50,51] Furthermore, LiF, which could be applied as a viable interlayer material to passivate the LLZO electrolyte,[13,52−54] exhibits substantially lower lithium-ion conductivity (~10^{-11} S/cm) than that of LLZOs.[3,55,56] It implies that LiF interlayer may exacerbate the imbalance of the lithium-ion flux distribution at the interface, thus was excluded. On the other hand, carbon-based material preliminarily satisfies all of the criteria mentioned above and was considered as one of the most suitable candidates. It was predicted that it would induce the lithium metal to plate preferentially between the interlayer and current collector and provide sufficiently high ionic conductivities to enable fast redistribution of lithium ions through interlayers.[57] Additionally, unlike alloying compounds, the morphology of interlayers is not likely to change significantly as the lithium uptake by carbon involves intercalation/deintercalation or adsorption/desorption,[58] which accompanies only marginal volume change. Indeed, recent investigations have shown the promise of several carbonaceous materials as a stable interlayer between lithium metal anodes and solid electrolytes,[27,59] while the underlying mechanism has not been fully elucidated, and its application to the full cell employing commercial-level cathodes has yet to be examined.

Kinetics of Lithium Precipitation and the Strategy to Guide Lithium Plating. Among various carbonaceous materials, graphitic and amorphous carbon types were

https://doi.org/10.1021/acsenergylett.2c02150
ACS Energy Lett. 2023, 8, 9−20

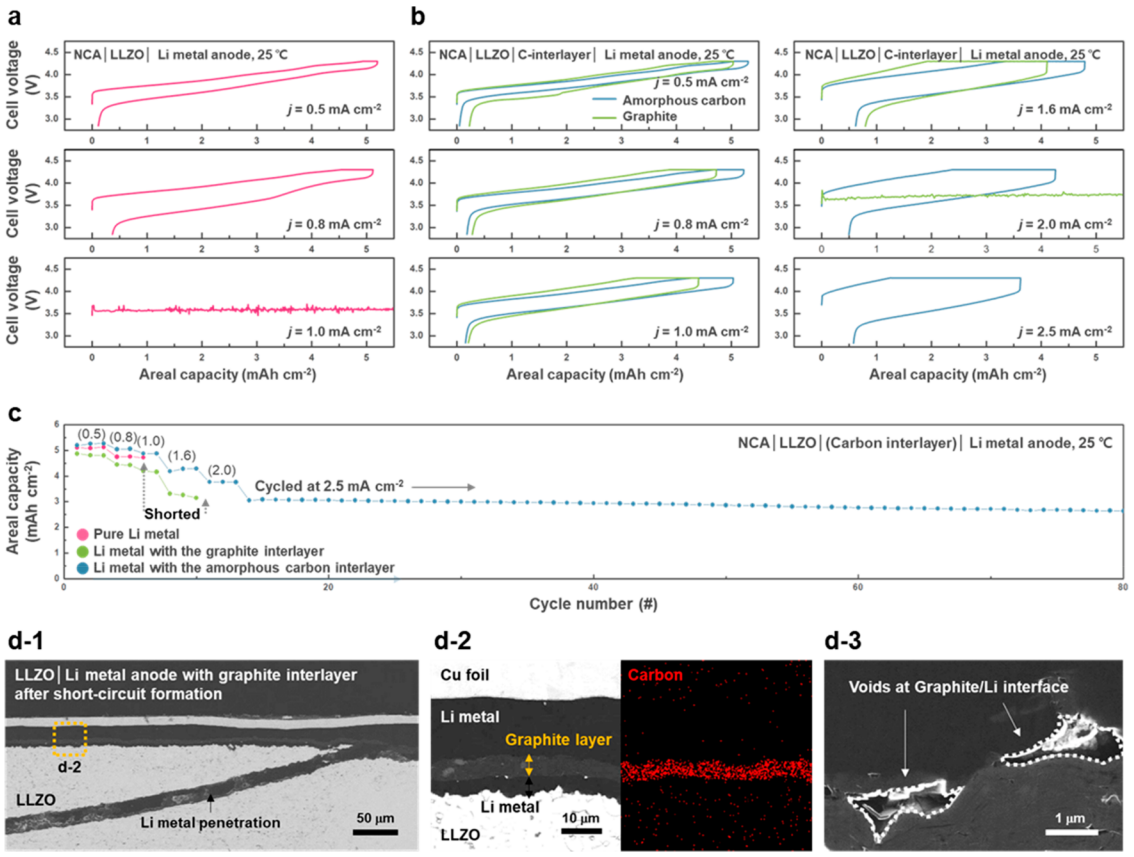

Figure 3. Comparisons of cell performances with or without interlayers. (a–c) Electrochemical performance of hybrid solid-state battery cells using garnet-type solid electrolytes and lithium–metal anodes with and without carbon interlayers, showing the significant differences in results due to the presence of the interlayer and the type of carbon. (d) Cross-sectional SEM and EDS images recorded after the failure of a cell with a graphite interlayer. Lithium metal was plated between the interlayer and the solid electrolyte, causing lithium penetration; voids were observed at the graphite layer/lithium metal interface.

investigated as model systems in this study. These two types of carbon were particularly selected as they can help unravel the relationships among carbon crystallinity, lithium transport property, and plating behavior.[58,60] The carbon interlayers were prepared by casting/drying of the slurry of carbon powder and polyvinylidene fluoride binder (93:7 (w/w)) dispersed in *N*-methyl-2-pyrrolidone (NMP) with approximately 3 μm of thickness (Figure S4, see the Experimental Section in the Supporting Information). In order to examine the lithium plating behavior through the carbon layer, an asymmetric half-cell was first prepared using lithium metal, LLZO pellet, and the current collector coated with the carbon interlayer assembled under 250 MPa using a cold isostatic press. In this electrochemical system, lithium was electrochemically stripped out from the lithium metal electrode and redeposited onto the opposite lithium-free electrode with the interlayer (Figure S5). Figure 2a illustrates the cross-sectional scanning electron microscopy (SEM) images of the interfaces with the energy dispersive X-ray spectroscopy (EDS) mapping after the lithium deposition on the interlayer-coated electrode. The electrochemical deposition was conducted at an elevated temperature (100 °C), a temperature at which the kinetic barrier can become sufficiently low, thereby enabling verification of the preferential lithium deposition positions as suggested from the interfacial energy calculations in Table 1. The figure clearly depicts that lithium was plated preferentially between the carbon interlayer and the current collector regardless of the type of carbon, as indicated by the arrows and dashed lines on the left and right panels, respectively. This is in agreement with our theoretical predictions from DFT calculations and supports the validity of selecting the interlayer materials based on the preferential lithium deposition position.

However, we found that lowering the operation temperature can significantly randomize the preferential lithium deposition positions. As presented in Figure 2b, the lithium metal was plated not only between the carbon and the current collector but also between the LLZO electrolyte and the carbon, notably deteriorating the original morphology of the carbon interlayer. This tendency was more pronounced for the graphite layer than the amorphous carbon layer. The discrepancy of the results at the low temperature strongly suggests that there is a competition between the thermodynamic-driven deposition preference and the lithium transport kinetics through the carbon interlayer. Since the lithium transport through the interlayer can become sluggish at lower temperatures (25 °C), the lithium plating at the remote positions may be kinetically hindered despite the energetic preference, making a randomized lithium deposition behavior. This speculation could be further supported by the similar experiment at 60 °C, at which the kinetics of lithium transport can be slightly more facile, as shown in Figure S6. At 60 °C, it was observed that the lithium metal could be readily precipitated at the carbon interlayer/current-collector interface particularly for the amorphous carbon interlayer as in the case of 100 °C, confirming that

https://doi.org/10.1021/acsenergylett.2c02150
ACS Energy Lett. 2023, 8, 9–20

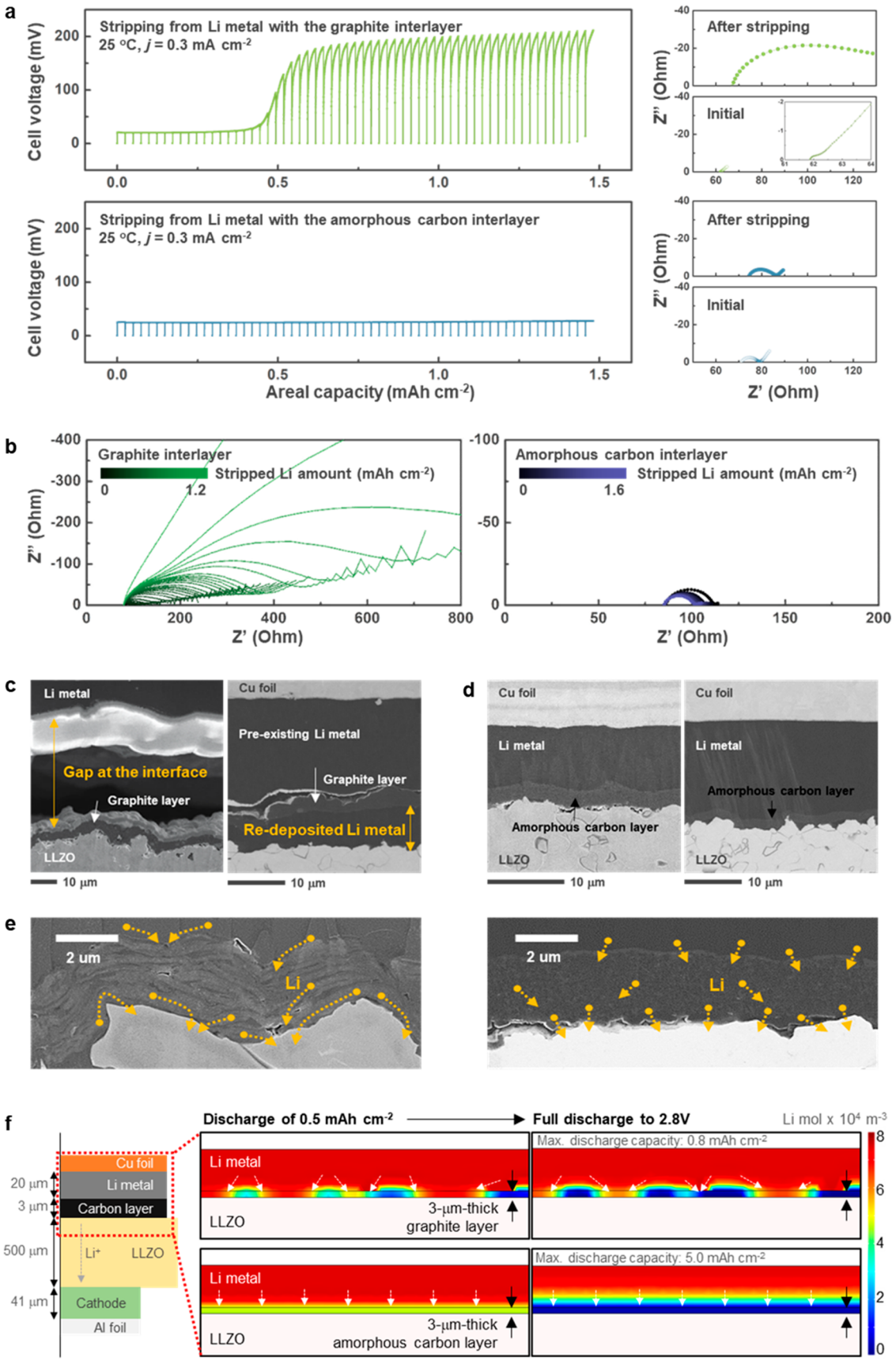

Figure 4. Influence of the lithium transport mechanism (according to the type of carbon) on lithium stripping behavior. (a) Voltage responses to the pulse currents as a function of the capacity during lithium stripping from the cell with (top) the graphite interlayer and (bottom) the amorphous carbon interlayer, and the EIS result of each cell before and after stripping. (b) Nyquist representations of the impedance-spectra evolutions on lithium stripping. (c, d) Cross-sectional SEM images of the LLZO solid electrolyte/lithium metal anode

https://doi.org/10.1021/acsenergylett.2c02150
ACS Energy Lett. 2023, 8, 9−20

Figure 4. continued

interface with the interlayers after lithium stripping and subsequent lithium plating. (e) SEM images of the particles in each interlayer indicating the dependence of the local lithium transport pathway on the orientation of particle alignment and crystallites of carbon (left, graphite; right, amorphous carbon). (f) Simulation of the consequent lithium concentration distribution with the lithium diffusion pathways (white arrows) in the anode with (top) the graphite interlayer and (bottom) the amorphous carbon interlayer during lithium stripping (e.g., discharging of the full cell with the configuration at the left side) at 2 mA cm^{-2}. (See Supporting Information Note S2 and Figure S11 for details).

the irregular lithium deposition was caused by the low temperature. Nevertheless, it was also noted that the lithium plating still partially occurred at the interlayer/LLZO electrolyte interface with the graphite case even at 60 °C, inferring that the intrinsic lithium diffusion property of the carbon may have a substantial influence. The aligned graphitic interlayer along the interface would not be favorable for the vertical lithium transport through the interlayer owing to the two-dimensional nature of lithium diffusion in graphite, which contrasts to the amorphous carbon with the nondirectional lithium diffusion property. This difference in the lithium transport would be also reflected in the high-current operation performance of the electrochemical system, as will be discussed further in detail later. Additionally, we could verify that the sluggish lithium nucleation kinetics was partly responsible for the randomized lithium deposition at the low temperature. In our comparative experiment, it was found that the preferential lithium deposition can be noticeably promoted even at the low temperature if a thin seed layer of lithium metal is simply added between the current collector and the interlayer (see the Supporting Information Experimental Section and Figure S5 for details). Figure 2c illustrates the cross-sectional SEM images of the sample with the thin seed layer inserted for the two cases of carbon interlayers. It evidently demonstrates that the lithium plating takes place onto the pre-existing lithium metal upon the electrochemical bias even at 25 °C regardless of the type of carbon (Figure S7), indicating that the absence of the nucleation step kinetically helps on the lithium precipitation at the thermodynamically favorable sites.[61]

Influence of the Carbon Interlayer on Cell Performance. Inspired by the stability of the carbon interlayer at the interface, a series of lithium cells were assembled using NCA811 ($LiNi_{0.8}Co_{0.1}Al_{0.1}O_2$) cathodes (with a capacity of 5.1 mAh cm^{-2} at 25 °C) and lithium metal anodes with graphite or amorphous carbon interlayer placed on LLZO electrolyte in comparisons to a bare lithium metal anode. The NCA811 cathode was soaked with a drop of liquid electrolyte for the cathode interface, whereas the lithium metal anode was interfaced only with the LLZO solid electrolyte with or without carbon interlayer. Panels a and b of Figure 3 comparatively present the charge/discharge curves of the hybrid solid-state cells without and with interlayer, respectively, cycled at increasing current densities from 0.5 to 2.5 mA cm^{-2}. It is observed that the NCA811/LLZO/Li cell without the interlayer exhibits a characteristic voltage profile of NCA811 at a relatively low current density (0.5 mA cm^{-2}); however, the polarization gets notably greater with a higher current density of 0.8 mA cm^{-2}, and it short-circuits at 1.0 mA cm^{-2}, which agrees with the previous observations.[44,45] On the other hand, the presence of the carbon interlayer allows a successful operation of the cell at considerably higher current densities. The cell with the graphite interlayer (green lines in Figure 3b) could sustain the current density of 1.6 mA cm^{-2}, delivering a reversible capacity of approximately 4 mAh cm^{-2}, while a higher current operation at 2 mA cm^{-2} caused a cell failure. More remarkable is that the employment of the amorphous carbon interlayer in the NCA811/LLZO/Li cell could further improve the cell stability. As presented with the blue lines in Figure 3b, the cells were capable of delivering appreciable capacities without cell failure at increasing rates from 0.5 to 2.5 mA cm^{-2}. Short-circuit signals such as voltage noise and/or sudden drop were not observable at a current density of as high as 2.5 mA cm^{-2}, exhibiting 70% retention of the initial capacity (5.2 mAh cm^{-2}) at 0.5 mA cm^{-2}. The cell could also display the extended cycle stability, as shown in Figure 3c, at 2.5 mA cm^{-2}, which did not exhibit any noticeable capacity degradations over 80 cycles.

It is noteworthy that the cells with the interlayer exhibited slightly different capacities and stabilities depending on the carbon types; e.g., the graphite interlayer cell delivered lower capacities (4.4 mAh cm^{-2} at 0.8 mA cm^{-2}, 4.2 mAh cm^{-2} at 1.0 mA cm^{-2}, and 3.3 mAh cm^{-2} at 1.6 mA cm^{-2}) than the cell with the amorphous interlayer (5.0 mAh cm^{-2} at 0.8 mA cm^{-2}, 4.9 mAh cm^{-2} at 1.0 mA cm^{-2}, and 4.3 mAh cm^{-2} at 1.6 mA cm^{-2}) and, more importantly, showed the earlier short-circuit formation at 2.0 mA cm^{-2}. We found that the difference in the performance was primarily caused by the durability of the carbon interlayer upon the repeated lithium stripping and deposition processes, similar to the observations in the half-cell experiments in Figure 2. Figure 3d illustrates a series of cross-sectional images of the NCA811/LLZO/Li cell with the graphite interlayer after the shortage, probing the interfacial region of LLZO/Li. Panel d-1l of Figure 3 clearly depict that the lithium metal has penetrated through the LLZO electrolyte (as indicated with a black arrow), causing the breakdown of the LLZO pellet. A closer view of this region (dotted line box) in Figure 3d-2 reveals that the lithium metal penetration into the electrolyte was linked with the lithium plating between the graphite interlayer and the LLZO electrolyte, which caused the direct contact between the lithium deposits and the LLZO electrolyte. Meanwhile, the interfaces formed by the amorphous carbon interlayer at LLZO/interlayer/lithium maintained the intimate physical contact even after cycling at high current densities (Figure S8). It suggests that the insufficient lithium transport property at the high current density could not guarantee the preferential lithium deposition at the interface of the LLZO/graphite interlayer, which is consistent with the observations of the kinetic limitations at the low temperature in Figure 2b. It was further observed that voids were formed at the graphite interlayer/lithium metal interface as shown in Figure 3d-3 and Figure S9, confirming the sluggish lithium transport through the graphite interlayer. Since the void formation is known to be related to the lithium stripping behavior,[20,21] it infers that the lithium transport through the interlayer, depending on the type of carbon, also influences the lithium stripping behavior as well as the lithium plating behavior, and eventually affects the cell performances.

https://doi.org/10.1021/acsenergylett.2c02150
ACS Energy Lett. 2023, 8, 9−20

Lithium Stripping through the Interlayer and the Orientation of Lithium Transport Pathways. In order to further elucidate the influence of the type of carbon in the interlayer, the kinetics of lithium transport through each interlayer was investigated regarding the lithium stripping process in the asymmetric half-cell (Figure S5). Figure 4a shows the overall voltage response curves of the lithium metal electrodes with the graphite or amorphous interlayer during lithium stripping under the same conditions (0.3 mA cm^{-2} at 25 °C) as a function of the amount of lithium stripped. Each curve was recorded over a series of current pulses (5 min each) and rest periods (115 min); the magnitude of the vertical line in cell voltage is the overpotential measured during the rest, which accounts for the resistance increase of the cell.[62] Notably, the cell with the graphite interlayer showed a significant increase in overpotential after ∼0.5 mAh cm^{-2} of lithium stripping, whereas the cell with the amorphous carbon interlayer showed a stable profile with a constantly low overpotential. A comparison of the electrochemical impedance spectroscopy (EIS) results before and after lithium stripping (Figure 4a right and Figure S10) indicated the increase is mainly attributed to the change in the interfacial resistance, and it is particularly greater in the cell with the graphite interlayer (from 0.4 Ω cm^2 to 60.8 Ω cm^2) than the case with the amorphous carbon, suggesting the deterioration of the graphite interface. The change in the impedance could be more clearly visualized from the galvanostatic electrochemical impedance spectroscopy (GEIS), which displays the real-time development of the interfacial resistance with the progress of stripping.[44] As shown in Figure 4b and Figure S11, the interfacial resistance gets gradually larger in the cell containing the graphite interlayer with the progress of lithium stripping (Figure 4a) and almost divulges at a higher degree of the stripping. It contrasts to a negligible change detected in the cell with the amorphous carbon interlayer.

The increase in the electrochemical impedance was observed to be coupled with the delamination of the interlayer, as validated with an SEM analysis in Figure 4c,d. The panels illustrate the cross-sectional images of the interfaces of the solid electrolyte and the lithium metal anode with the graphite (Figure 4c) or the amorphous carbon (Figure 4d) interlayers after the stripping (left-hand-side images) and the subsequent lithium plating (right-hand-side images). We found that a large gap was generated after the lithium stripping at the graphite interlayer/lithium metal interface, which was extensively observed throughout the sample. It is generally known to be detrimental, inhibiting the effective lithium transport, and substantially increases the cell resistance, in a remarkable consistency with the observations in the EIS analysis. On the other hand, the interfaces formed by the amorphous carbon interlayer at LLZO/interlayer/lithium maintained the intimate physical contact throughout the stripping process. Moreover, it was observed that the subsequent lithium plating could be considerably affected by the distinct stripping behaviors of the two cases. The right-hand-side image of Figure 4c shows that the redeposition of lithium takes place primarily at the interface between the LLZO and the graphite layer due to the presence of the gap that disconnects the current collector, which further aggravates the delamination of the interlayer from the LLZO. On the contrary, in the cell with the amorphous carbon interlayer, lithium could be replated on the pre-existing lithium metal through the interlayer, which continues to aid in the preferential plating after lithium stripping due to its morphological stability.

We suppose that the distinct behaviors of the two interlayers are attributable to the different lithium transport pathways arising from the crystallographic characteristics of each material (Figure S12). Graphite is constructed by stackings of graphene basal planes, within which lithium ions diffuse via intercalation/deintercalation mechanism.[63] This two-dimensional lithium transport behavior provides anisotropic pathways of lithium ions in the interlayer containing graphite platelets with the preferred orientations, as schematically illustrated in Figure 4e. It may cause non-uniform current distribution at the graphite interlayer/lithium metal interface under kinetically challenging conditions such as at low temperature and high current rates, which eventually leads to localized lithium stripping. On the other hand, amorphous carbon can offer the isotropic lithium transport pathways due to its highly disordered structure and the transport mechanisms involving surface adsorption/desorption and lithium cluster storage in nanopores.[58,60] The three-dimensional lithium transport (without preference for a specific direction) would lead to a uniform current distribution through the amorphous carbon interlayer and at the interlayer/lithium metal interface. We could also confirm that this inhomogeneity of lithium transport is consistently observable in the measurements of apparent lithium diffusivities through each carbon interlayer. In Figure S13, the diffusion coefficients of lithium were estimated for each carbon layer during delithiation using a galvanostatic intermittent titration technique (GITT).[62,64] It presents that the lithium diffusivity in the graphite interlayer remains lower than that in the amorphous interlayer, contradictory to the higher intrinsic lithium diffusivity in graphite than in soft carbons or hard carbons.[57] It is because of the geometric texture of the graphite interlayer with the preferred orientations of graphite platelets and implies that the directionality of lithium transport in the interlayer can have a considerable effect on the overall performance. The influence of anisotropic lithium transport could be further validated by computational simulations, as shown in Figure 4f and Figure S14. The continuum mechanics simulations (see SI Note S2, Figure S14, and Table S2) could analyze the spatial distribution of lithium concentration near the region of the interlayer and lithium−metal electrode during the stripping process.[65] Considering the textured basal planes of the graphite,[63] the interfaces formed with the lithium metal or LLZO electrolyte were set to be partially activated/available for lithium transport. It illustrates that the lithium concentration evolves uniformly with the amorphous carbon interlayer, delivering a desired discharge capacity of 5 mAh cm^{-2} at 2 mA cm^{-2}, whereas inhomogeneous lithium distributions developed in the cell using the graphite interlayer with a limited capacity lower than 1 mAh cm^{-2} at the same current density. This result confirms that the non-uniform current distribution that arises from the anisotropic lithium transport in the interlayer can cause a detrimental effect on the cell performance.

Optimization of Amorphous Carbon Interlayer for LLZO Electrolyte. Based on the understandings of the lithium plating/stripping behaviors depending on carbon types, we further optimized the amorphous carbon interlayer for the enhanced lithium transport and tested its applicability in the following. As the isotropic lithium transport in the carbon

https://doi.org/10.1021/acsenergylett.2c02150
ACS Energy Lett. 2023, 8, 9−20

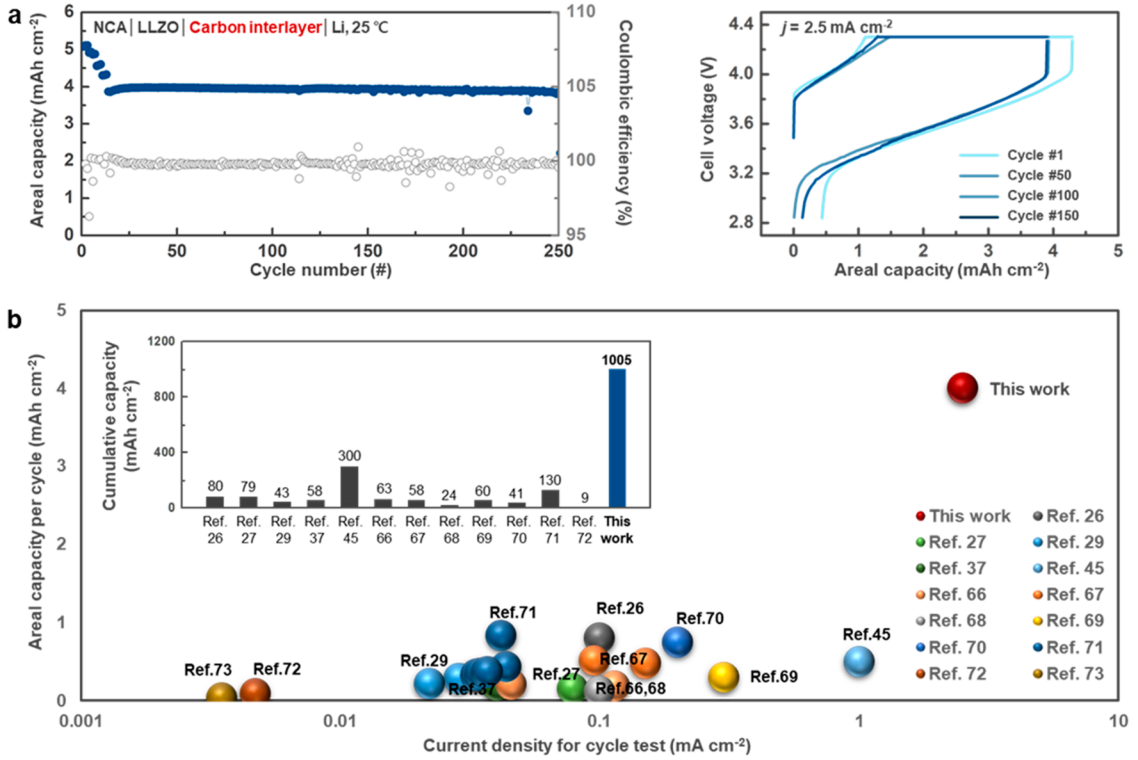

Figure 5. Outstanding performance of the cell using the optimized amorphous carbon interlayer. (a) Long-term cycling performance of the NCA811/LLZO/amorphous carbon interlayer/lithium−metal cell. The cell maintained stable cycling performance over 250 cycles, generating 4.0 mAh cm^{-2} at 2.5 mA cm^{-2} without significant degradation of the capacity. The initial 13 precycles were conducted at 0.5, 0.8, 1.0, 1.6, and 2 mA cm^{-2}, respectively, before cycling at 2.5 mA cm^{-2}. (b) Performance comparison of solid-state batteries using garnet-type solid electrolytes and lithium−metal anodes. The plot summarizes the current densities (x-axis) and areal plating capacities of cathodes (y-axis) reported previously.[26,27,29,37,45,66−73] The inset graph compares the cumulative areal capacities of lithium plating (the number at the top of each bar) of full cells.

interlayer is important in the uniform current distribution, we adopted the amorphous carbon, of which the particle and crystallite size is smaller (Figure S15). Considering that lithium transport in amorphous carbon occurs through the surface interactions,[58,60] this small-sized amorphous carbon was expected to provide more effective lithium transport pathways. Accordingly, a portion of the small-sized carbon particles was added to the original amorphous carbon interlayer with the weight fraction of 25%, and a hybrid solid-state lithium cell was assembled employing NCA811 cathode. Figure 5a presents the electrochemical performance of the cell tested in the practical battery conditions of high current density (2.5 mA cm^{-2}) and areal capacity (5.1 mAh cm^{-2}) at CCCV (constant current and constant voltage) mode within the 2.8−4.3 V region at 25 °C (see the SI Experimental Section for details). The cell exhibits a remarkable cycling performance over 250 cycles at 2.5 mA cm^{-2} without significant capacity degradation or short-circuit failure, after the initial precycles. The capacity retention is as high as 99.6% after 250 cycles, presenting an extraordinarily high cycle stability. Moreover, the change in the electrochemical profiles was markedly small throughout the cycles, indicating the robustness of the cell. For comparisons with other solid-state cells employing LLZO electrolyte that have been reported, we plotted a performance map of solid-state lithium metal cells in terms of important practical parameters of current density and areal capacity in Figure 5b. Notably, the state-of-the-art cell reported to date implements a cathode with an areal capacity less than 1.0 mAh cm^{-2}, which is not applicable for practical battery systems. On the other hand, our system adopts the cathode of 5.1 mAh cm^{-2} areal capacity, which meets the industrial standard. The cumulative lithium capacities were calculated and depicted in the inset of the graph, summing up the delivered capacity of the lithium metal anodes through the cycles in the full cells. It records 1005 mAh cm^{-2}, which are significantly higher than other reported values.[26,27,29,37,45,66−73] To the best of our knowledge, these are the highest values reported for solid-state lithium metal cells that were operated at 25 °C employing garnet-type oxide electrolytes and lithium metal anodes. This outstanding performance demonstration is expected to pave a new pathway toward the development of practical-level all-solid-state-batteries, and highlights the importance of the interlayer design/stability not only ensuring the intimate contact but also regulating the lithium transport path in relation with the crystalline domain orientations for current redistribution, thus warranting further future research.

A high-power solid-state lithium metal battery capable of stable room temperature operation was successfully constructed by introducing an optimal interlayer at the interface of a lithium metal anode and an LLZO solid electrolyte. This interlayer was designed through a systematic investigation of the role of the interlayer on lithium plating/stripping behavior using theoretical and experimental analyses. Based on the thermodynamic properties of the candidate materials, a carbon-based material was selected as the most suitable material for an ideal interlayer, which can induce lithium plating between the current collector (copper) and the interlayer without significant physical/chemical changes. It

https://doi.org/10.1021/acsenergylett.2c02150
ACS Energy Lett. 2023, 8, 9−20

was also shown that preferential lithium plating between the interlayer and the current collector can be effectively facilitated by the introduction of a thin seed layer of lithium metal, which can effectively lower the high kinetic energy barrier for lithium nucleation. Moreover, the critical impact of the crystalline orientation of the graphitic carbon on the stability of interlayer was elucidated by showing that the amorphous carbon interlayer, which can provide isotropic lithium transport (without preference for a specific direction), could maintain its original interlayer/lithium metal interface after the repeated lithium plating/stripping, in contrast to the case of the graphite interlayer. A full cell utilizing an optimal amorphous carbon interlayer presented excellent performance, with a cumulative lithium metal capacity of over 1000 mAh cm^{-2} at 2.5 mA cm^{-2} at room temperature. This is the first report of a potential high-power solid-state lithium metal battery at a commercial-level, successfully operating without short-circuiting, and validates the efficacy of the interlayer designing strategy described here. Although other requirements such as fast and/or low-temperature charging should be further examined in the future, the findings in this study are expected to open new frontiers in the development of solid-state batteries by providing the critical keys to ensure the stable interface between lithium anode and the oxide-based electrolyte.

■ ASSOCIATED CONTENT

Supporting Information

The Supporting Information is available free of charge at https://pubs.acs.org/doi/10.1021/acsenergylett.2c02150.

Experimental details of LLZO electrolyte pellets preparation and of materials characterizations; interlayer fabrication; cell assembly and electrochemical test conditions; details of calculations; additional characterization and electrochemical test results (Figures S1−S15 and Tables S1 and S2) (PDF)

■ AUTHOR INFORMATION

Corresponding Author

Kisuk Kang − *Department of Materials Science and Engineering, Center for Nanoparticle Research, Institute of Basic Science (IBS), Institute of Engineering Research, College of Engineering, and School of Chemical and Bioengineering, College of Engineering, Seoul National University, Seoul 08826, Republic of Korea;* orcid.org/0000-0002-8696-1886; Email: matlgen1@snu.ac.kr

Authors

Sewon Kim − *Department of Materials Science and Engineering, Seoul National University, Seoul 08826, Republic of Korea; Battery Material Lab, Samsung Advanced Institute of Technology, Suwon-si, Gyeonggi-do 16678, Republic of Korea;* orcid.org/0000-0002-3886-8898

Gabin Yoon − *Battery Material Lab, Samsung Advanced Institute of Technology, Suwon-si, Gyeonggi-do 16678, Republic of Korea*

Sung-Kyun Jung − *Department of Energy Engineering, School of Energy and Chemical Engineering, Ulsan National Institute of Science and Technology (UNIST), Ulsan 44919, Republic of Korea;* orcid.org/0000-0002-3708-3757

SeonTae Park − *Analytical Engineering Group, Samsung Advanced Institute of Technology, Suwon-si, Gyeonggi-do 16678, Republic of Korea*

Ju-Sik Kim − *Battery Material Lab, Samsung Advanced Institute of Technology, Suwon-si, Gyeonggi-do 16678, Republic of Korea*

Kyungho Yoon − *Department of Materials Science and Engineering, Seoul National University, Seoul 08826, Republic of Korea*

Sunyoung Lee − *Department of Materials Science and Engineering, Seoul National University, Seoul 08826, Republic of Korea*

Complete contact information is available at: https://pubs.acs.org/10.1021/acsenergylett.2c02150

Author Contributions

○S.K. and G.Y. contributed equally to this work.

Notes

The authors declare no competing financial interest.

■ ACKNOWLEDGMENTS

This research was supported by the National Research Foundation of Korea (NRF) grant funded by the Korea government (NRF-2021M3H4A1A04093047), and Samsung Advanced Institute of Technology, Samsung Electronics Co., Ltd.

■ REFERENCES

(1) Janek, J.; Zeier, W. G. A solid future for battery development. *Nat. Energy* **2016**, *1*, 16141.

(2) Manthiram, A.; Yu, X.; Wang, S. Lithium battery chemistries enabled by solid-state electrolytes. *Nat. Rev. Mater.* **2017**, *2*, 16103.

(3) Samson, A. J.; Hofstetter, K.; Bag, S.; Thangadurai, V. A bird's-eye view of Li-stuffed garnet-type Li7La3Zr2O12 ceramic electrolytes for advanced all-solid-state Li batteries. *Energy Environ. Sci.* **2019**, *12*, 2957−2975.

(4) Sun, C.; Liu, J.; Gong, Y.; Wilkinson, D. P.; Zhang, J. Recent advances in all-solid-state rechargeable lithium batteries. *Nano Energy* **2017**, *33*, 363−386.

(5) Kim, S.; et al. *Role of Interlayer Chemistry in Li-Metal Growth through a Garnet-Type Solid Electrolyte* **2020**, *10*, 1903993.

(6) Kim, S.; et al. High-energy and durable lithium metal batteries using garnet-type solid electrolytes with tailored lithium-metal compatibility. *Nat. Commun.* **2022**, *13*, 1883.

(7) Sharafi, A.; et al. Surface Chemistry Mechanism of Ultra-Low Interfacial Resistance in the Solid-State Electrolyte Li7La3Zr2O12. *Chem. Mater.* **2017**, *29*, 7961−7968.

(8) Miara, L. J.; et al. Effect of Rb and Ta Doping on the Ionic Conductivity and Stability of the Garnet Li7 + 2x−y(La3−xRbx)(Zr2−yTay)O12 ($0 \leq x \leq 0.375$, $0 \leq y \leq 1$) Superionic Conductor: A First Principles Investigation. *Chem. Mater.* **2013**, *25*, 3048−3055.

(9) Li, Y.; Han, J.-T.; Wang, C.-A.; Xie, H.; Goodenough, J. B. Optimizing Li+ conductivity in a garnet framework. *J. Mater. Chem.* **2012**, *22*, 15357−15361.

(10) Murugan, R.; Thangadurai, V.; Weppner, W. Fast Lithium Ion Conduction in Garnet-Type Li7La3Zr2O12. *Angew. Chem., Int. Ed.* **2007**, *46*, 7778−7781.

(11) Zhu, Y.; He, X.; Mo, Y. Origin of Outstanding Stability in the Lithium Solid Electrolyte Materials: Insights from Thermodynamic Analyses Based on First-Principles Calculations. *ACS Appl. Mater. Interfaces* **2015**, *7*, 23685−23693.

(12) Cheng, E. J.; Sharafi, A.; Sakamoto, J. Intergranular Li metal propagation through polycrystalline Li6.25Al0.25La3Zr2O12 ceramic electrolyte. *Electrochim. Acta* **2017**, *223*, 85−91.

(13) Aguesse, F.; et al. Investigating the Dendritic Growth during Full Cell Cycling of Garnet Electrolyte in Direct Contact with Li Metal. *ACS Appl. Mater. Interfaces* **2017**, *9*, 3808−3816.

(14) Sharafi, A.; Meyer, H. M.; Nanda, J.; Wolfenstine, J.; Sakamoto, J. Characterizing the Li−Li7La3Zr2O12 interface stability and kinetics as a function of temperature and current density. *J. Power Sources* **2016**, *302*, 135−139.
(15) Swamy, T.; et al. Lithium Metal Penetration Induced by Electrodeposition through Solid Electrolytes: Example in Single-Crystal Li6La3ZrTaO12 Garnet. *J. Electrochem. Soc.* **2018**, *165*, A3648−A3655.
(16) Porz, L.; et al. Mechanism of lithium metal penetration through inorganic solid electrolytes. *Adv. Energy Mater.* **2017**, *7*, 1701003.
(17) Han, F.; et al. High electronic conductivity as the origin of lithium dendrite formation within solid electrolytes. *Nat. Energy* **2019**, *4*, 187−196.
(18) Liu, X.; et al. Local electronic structure variation resulting in Li 'filament' formation within solid electrolytes. *Nat. Mater.* **2021**, *20*, 1485.
(19) Tsai, C.-L.; et al. Li7La3Zr2O12 Interface Modification for Li Dendrite Prevention. *ACS Appl. Mater. Interfaces* **2016**, *8*, 10617−10626.
(20) Krauskopf, T.; Hartmann, H.; Zeier, W. G.; Janek, J. Toward a Fundamental Understanding of the Lithium Metal Anode in Solid-State Batteries—An Electrochemo-Mechanical Study on the Garnet-Type Solid Electrolyte Li6.25Al0.25La3Zr2O12. *ACS Appl. Mater. Interfaces* **2019**, *11*, 14463−14477.
(21) Kasemchainan, J.; et al. Critical stripping current leads to dendrite formation on plating in lithium anode solid electrolyte cells. *Nat. Mater.* **2019**, *18*, 1105−1111.
(22) Ning, Z.; et al. Visualizing plating-induced cracking in lithium-anode solid-electrolyte cells. *Nat. Mater.* **2021**, *20*, 1121.
(23) Krauskopf, T.; Richter, F. H.; Zeier, W. G.; Janek, J. Physicochemical Concepts of the Lithium Metal Anode in Solid-State Batteries. *Chem. Rev.* **2020**, *120*, 7745−7794.
(24) Koshikawa, H.; et al. Dynamic changes in charge-transfer resistance at Li metal/Li7La3Zr2O12 interfaces during electrochemical Li dissolution/deposition cycles. *J. Power Sources* **2018**, *376*, 147−151.
(25) Han, X.; et al. Negating interfacial impedance in garnet-based solid-state Li metal batteries. *Nat. Mater.* **2017**, *16*, 572.
(26) Luo, W.; et al. Reducing Interfacial Resistance between Garnet-Structured Solid-State Electrolyte and Li-Metal Anode by a Germanium Layer. *Adv. Mater.* **2017**, *29*, 1606042.
(27) Shao, Y.; et al. Drawing a Soft Interface: An Effective Interfacial Modification Strategy for Garnet-Type Solid-State Li Batteries. *ACS Energy Lett.* **2018**, *3*, 1212−1218.
(28) Luo, W.; et al. Transition from Superlithiophobicity to Superlithiophilicity of Garnet Solid-State Electrolyte. *J. Am. Chem. Soc.* **2016**, *138*, 12258−12262.
(29) Huo, H.; et al. In-situ formed Li2CO3-free garnet/Li interface by rapid acid treatment for dendrite-free solid-state batteries. *Nano Energy* **2019**, *61*, 119−125.
(30) Ferraresi, G.; Uhlenbruck, S.; Tsai, C.-L.; Novák, P.; Villevieille, C. Engineering of Sn and Pre-Lithiated Sn as Negative Electrode Materials Coupled to Garnet Ta-LLZO Solid Electrolyte for All-Solid-State Li Batteries. *Batteries Supercaps* **2020**, *3*, 557−565.
(31) Feng, W.; Dong, X.; Li, P.; Wang, Y.; Xia, Y. Interfacial modification of Li/Garnet electrolyte by a lithiophilic and breathing interlayer. *J. Power Sources* **2019**, *419*, 91−98.
(32) Feng, W.; et al. Building an Interfacial Framework: Li/Garnet Interface Stabilization through a Cu6Sn5 Layer. *ACS Energy Lett.* **2019**, *4*, 1725−1731.
(33) He, M.; Cui, Z.; Chen, C.; Li, Y.; Guo, X. Formation of self-limited, stable and conductive interfaces between garnet electrolytes and lithium anodes for reversible lithium cycling in solid-state batteries. *J. Mater. Chem. A* **2018**, *6*, 11463−11470.
(34) Meng, J.; Zhang, Y.; Zhou, X.; Lei, M.; Li, C. Li2CO3-affiliative mechanism for air-accessible interface engineering of garnet electrolyte via facile liquid metal painting. *Nat. Commun.* **2020**, *11*, 3716.
(35) Wang, C.; et al. Conformal, Nanoscale ZnO Surface Modification of Garnet-Based Solid-State Electrolyte for Lithium Metal Anodes. *Nano Lett.* **2017**, *17*, 565−571.
(36) Lou, J.; et al. Achieving efficient and stable interface between metallic lithium and garnet-type solid electrolyte through a thin indium tin oxide interlayer. *J. Power Sources* **2020**, *448*, 227440.
(37) Huo, H.; et al. Design of a mixed conductive garnet/Li interface for dendrite-free solid lithium metal batteries. *Energy Environ. Sci.* **2020**, *13*, 127−134.
(38) Zhong, Y.; et al. A Highly Efficient All-Solid-State Lithium/Electrolyte Interface Induced by an Energetic Reaction. *Angew. Chem., Int. Ed.* **2020**, *59*, 14003−14008.
(39) Baniya, A.; et al. Mitigating Interfacial Mismatch between Lithium Metal and Garnet-Type Solid Electrolyte by Depositing Metal Nitride Lithiophilic Interlayer. *ACS Appl. Energy Mater.* **2022**, *5*, 648−657.
(40) Ruan, Y.; et al. A 3D Cross-Linking Lithiophilic and Electronically Insulating Interfacial Engineering for Garnet-Type Solid-State Lithium Batteries. *Adv. Funct. Mater.* **2021**, *31*, 2007815.
(41) Tang, S.; et al. Modifying an ultrathin insulating layer to suppress lithium dendrite formation within garnet solid electrolytes. *J. Mater. Chem. A* **2021**, *9*, 3576−3583.
(42) Cui, C.; et al. One-step fabrication of garnet solid electrolyte with integrated lithiophilic surface. *Energy Storage Mater.* **2022**, *45*, 814−820.
(43) Huang, Y.; et al. Graphitic Carbon Nitride (g-C3N4): An Interface Enabler for Solid-State Lithium Metal Batteries. *Angew. Chem., Int. Ed.* **2020**, *59*, 3699−3704.
(44) Krauskopf, T.; Mogwitz, B.; Rosenbach, C.; Zeier, W. G.; Janek, J. Diffusion Limitation of Lithium Metal and Li−Mg Alloy Anodes on LLZO Type Solid Electrolytes as a Function of Temperature and Pressure. *Adv. Energy Mater.* **2019**, *9*, 1902568.
(45) Lee, K.; et al. Multifunctional Interface for High-Rate and Long-Durable Garnet-Type Solid Electrolyte in Lithium Metal Batteries. *ACS Energy Lett.* **2022**, *7*, 381−389.
(46) Huggins, R. A. *Advanced Batteries: Materials Science Aspects*; Springer: New York, NY, 2009. DOI: 10.1007/978-0-387-76424-5.
(47) Chou, C.-Y.; Kim, H.; Hwang, G. S. A Comparative First-Principles Study of the Structure, Energetics, and Properties of Li−M (M = Si, Ge, Sn) Alloys. *J. Phys. Chem. C* **2011**, *115*, 20018−20026.
(48) Yan, K.; et al. Selective deposition and stable encapsulation of lithium through heterogeneous seeded growth. *Nat. Energy* **2016**, *1*, 16010.
(49) Kim, S. Y.; Li, J. Porous Mixed Ionic Electronic Conductor Interlayers for Solid-State Batteries. *Energy Mater. Adv.* **2021**, *2021*, 1519569.
(50) Li, H.; et al. Circumventing huge volume strain in alloy anodes of lithium batteries. *Nat. Commun.* **2020**, *11*, 1584.
(51) Jin, S.; et al. Solid−Solution-Based Metal Alloy Phase for Highly Reversible Lithium Metal Anode. *J. Am. Chem. Soc.* **2020**, *142*, 8818−8826.
(52) Tian, H.-K.; Xu, B.; Qi, Y. Computational study of lithium nucleation tendency in Li7La3Zr2O12 (LLZO) and rational design of interlayer materials to prevent lithium dendrites. *J. Power Sources* **2018**, *392*, 79−86.
(53) Song, Y.; et al. Revealing the Short-Circuiting Mechanism of Garnet-Based Solid-State Electrolyte. *Adv. Energy Mater.* **2019**, *9*, 1900671.
(54) Song, Y.; et al. Probing into the origin of an electronic conductivity surge in a garnet solid-state electrolyte. *J. Mater. Chem. A* **2019**, *7*, 22898−22902.
(55) Pan, J.; Cheng, Y.-T.; Qi, Y. General method to predict voltage-dependent ionic conduction in a solid electrolyte coating on electrodes. *Phys. Rev. B* **2015**, *91*, 134116.
(56) Oi, T. Ionic conductivity of LiF thin films containing Di- or trivalent metal fluorides. *Mater. Res. Bull.* **1984**, *19*, 451−457.
(57) Guo, H.-j.; et al. Diffusion coefficient of lithium in artificial graphite, mesocarbon microbeads, and disordered carbon. *New Carbon Mater.* **2007**, *22*, 7−10.

(58) Dahn, J. R.; Zheng, T.; Liu, Y.; Xue, J. S. Mechanisms for Lithium Insertion in Carbonaceous Materials. *Science* **1995**, *270*, 590.
(59) Suzuki, N.; et al. Highly Cyclable All-Solid-State Battery with Deposition-Type Lithium Metal Anode Based on Thin Carbon Black Layer. *Adv. Energy Sustainability Res.* **2021**, *2*, 2100066.
(60) Buiel, E.; Dahn, J. R. Li-insertion in hard carbon anode materials for Li-ion batteries. *Electrochim. Acta* **1999**, *45*, 121−130.
(61) Porter, D. A.; Easterling, K. E.; Sherif, M. Y. *Phase Transformations in Metals and Alloys (Revised Reprint)*, 3rd ed.; CRC Press, 2009.
(62) Weppner, W.; Huggins, R. A. Determination of the Kinetic Parameters of Mixed-Conducting Electrodes and Application to the System Li3Sb. *J. Electrochem. Soc.* **1977**, *124*, 1569−1578.
(63) Persson, K.; et al. Lithium Diffusion in Graphitic Carbon. *J. Phys. Chem. Lett.* **2010**, *1*, 1176−1180.
(64) Wen, C. J.; Boukamp, B. A.; Huggins, R. A.; Weppner, W. Thermodynamic and Mass Transport Properties of " LiAl". *J. Electrochem. Soc.* **1979**, *126*, 2258−2266.
(65) Yoon, G.; Moon, S.; Ceder, G.; Kang, K. Deposition and Stripping Behavior of Lithium Metal in Electrochemical System: Continuum Mechanics Study. *Chem. Mater.* **2018**, *30*, 6769−6776.
(66) Huo, H.; et al. A flexible electron-blocking interfacial shield for dendrite-free solid lithium metal batteries. *Nat. Commun.* **2021**, *12*, 176.
(67) Ruan, Y.; et al. Acid induced conversion towards a robust and lithiophilic interface for Li−Li7La3Zr2O12 solid-state batteries. *J. Mater. Chem. A* **2019**, *7*, 14565−14574.
(68) Xu, H.; et al. Li3N-Modified Garnet Electrolyte for All-Solid-State Lithium Metal Batteries Operated at 40 °C. *Nano Lett.* **2018**, *18*, 7414−7418.
(69) Chen, H.; et al. Improved Interface Stability and Room-Temperature Performance of Solid-State Lithium Batteries by Integrating Cathode/Electrolyte and Graphite Coating. *ACS Appl. Mater. Interfaces* **2020**, *12*, 15120−15127.
(70) Su, J.; et al. Overcoming the abnormal grain growth in Ga-doped Li7La3Zr2O12 to enhance the electrochemical stability against Li metal. *Ceram. Int.* **2019**, *45*, 14991−14996.
(71) Chen, S.; et al. All-Solid-State Batteries with a Limited Lithium Metal Anode at Room Temperature using a Garnet-Based Electrolyte. *Adv. Mater.* **2021**, *33*, 2002325.
(72) Han, F.; et al. Interphase Engineering Enabled All-Ceramic Lithium Battery. *Joule* **2018**, *2*, 497−508.
(73) Ohta, S.; Kobayashi, T.; Seki, J.; Asaoka, T. Electrochemical performance of an all-solid-state lithium ion battery with garnet-type oxide electrolyte. *J. Power Sources* **2012**, *202*, 332−335.

https://doi.org/10.1021/acsenergylett.2c02150
ACS Energy Lett. 2023, 8, 9−20